



Solid-core photonic crystal fiber-based nanolayer glucose sensor

Malik J. Abd-ALhussain¹ · Bassam G. Rasheed¹ ·
Makram A. Fakhri²

Received: 13 July 2023 / Accepted: 7 September 2023 / Published online: 5 October 2023
© The Author(s), under exclusive licence to The Optical Society of India 2023

Abstract In this article, a solid-core photonic crystal fiber was developed to examine different concentrations and refractive indices of dissolved glucose in water and blood samples using surface plasmon resonance. A photonic crystal fiber with coated sensor model based on (gold and silver) nanolayer was proposed. The experimental results exhibit a sensitivity of 1943.43 nm/RIU and 1892.18 nm/RIU for samples with glucose concentrations in water ranging from 80 mg/dl to 600 mg/dl when PCF is coated with gold and silver nanofilm, respectively. It also exhibits wavelength sensitivity of 1114.164 nm/RIU and 1012.364 nm/RIU for glucose concentrations in blood serum at range from 89 mg/dl to 611 mg/dl using PCF coated with identical 50 nm thick gold and silver nanofilms, respectively. It is found that the maximum resolution of the proposed PCF was 3.3×10^{-5} .

Keywords Photonic crystal fiber · PCF sensor · Surface plasmonic resonance

Introduction

Photonic Crystal Fiber (PCF), also known as a microstructure optical fiber, is a particular type of optical fiber with a periodic arrangement of air holes running along its length, forming a photonic crystal structure [1, 2]. Based on their internal structure, PCFs can also be divided into types,

solid-core and hollow-core PCFs [3–6]. In solid-core fibers, light is confined to the core by total internal reflection, and in hollow-core fibers, the light is confined by the photonic bandgap of the cladding material [7, 8]. Photonic crystal fibers (PCFs) have excellent performance, including endless single-mode transmission, chromatic dispersion, controllable birefringence, and high nonlinearity, and have been widely applied and become a recent focus in the field of optical devices [9, 10].

Optical sensors have garnered significant attention due to their ability to detect biochemical molecules, external environmental conditions, refractive index (RI), temperature, magnetic fields, pressure, and various ambient properties in real time. The evanescent field coupling technique has emerged to enhance sensitivity toward the surrounding medium. Building upon this concept, researchers have proposed using surface plasmon resonance (SPR)-based photonic crystal fibers (PCFs) [11–14].

Due to its sensitivity to the permittivity of the environment, surface plasmon resonance (SPR) is regarded as an excellent method for detecting minor refractive index (RI) variations. SPR sensors are often used in chemical and physical senses due to their increased sensitivity and real-time detection [15–18]. Numerous SPR-based PCF refractive index sensors have been investigated over the last years for further advancement of PCF sensing technology. Surface plasmon waves are short-lived waves made when electrons and photons resonate at the same frequency on the surface of a metal. During the transmission process, this type of wave is sensitive to the environment outside [19–22]. PCF-SPR sensors can be divided into two groups: internally nanometal-coated and externally nanometal-coated PCF sensors [23, 24].

A relatively effective plasmonic material is thought to be gold nanomaterial. Moreover, it is believed to be

✉ Makram A. Fakhri
makram.a.fakhri@uotechnology.edu.iq;
mokaram_76@yahoo.com

¹ Laser and Optoelectronic Engineering Department College of Engineering, Al Nahrain University, Baghdad, Iraq

² Laser and Optoelectronic Department, University of Technology-Iraq, Baghdad, Iraq

chemically stable and unaffected by the immediate oxidation issue [25–28]. Due to the quantum confinement effect, gold nanoparticles have more negative Fermi potentials and a larger absorption band than other materials. Given that Au-NPs have a higher refractive index than silica optical fiber, the guided light would couple into Au-NPs waveguides [29, 30]. Due to their unique optical properties, silver nanoparticles are often used as plasmon resonance material in Surface Plasmon Resonance (SPR) sensors [31, 32]. When light interacts with metal nanoparticles, such as silver nanoparticles, the collective oscillation of conduction electrons leads to the generation of a surface plasmon wave, known as surface plasmon resonance (SPR). SPR can occur in various metal nanoparticles, including silver and gold. The resonance in SPR refers to the condition where the incident light matches the frequency at which the surface plasmon wave is most efficiently excited. This results in strong absorption and scattering of light, which is highly sensitive to changes in the surrounding environment. Silver shows a sharper resonance peak compared to the other plasmonic materials [33–36]. Researchers are now very interested in designing unique structures and enhancing the performance characteristics of SPR-based PCF sensors because they can be used in a variety of fields, such as medical diagnostics, bio-sensing, gas detection, water testing, glucose monitoring, bio-imaging [37, 38], virus detection [39, 40], drug testing [41, 42], biotechnology, and chemical sensing [43, 44].

Theory

When an electromagnetic wave interacts with a metal–dielectric interface, maximum optical energy is transferred to surface electronic oscillations on the metal, creating surface plasmons at resonance conditions. By introducing the right wavelength of the electromagnetic wave into a suitably oriented photonic crystal fiber (PCF) waveguide, surface plasmon waves (SPWs) can be generated and propagating forward along the interface. The propagation constant β_{SPR} of SPR expresses as [45–48]:

$$\beta_{\text{SPR}} = \frac{\omega}{c} \left(\sqrt{\frac{\epsilon_m \epsilon_s}{\epsilon_m + \epsilon_s}} \right) \tag{1}$$

where c is the speed of light in vacuum, ω is the angular frequency of the light, ϵ_m and ϵ_s are the relative permittivity of the metal film and the surrounding material adjacent to the metal interface where the surface plasmon polariton (SPP) is located, respectively. The V-number and the Numerical Aperture (NA) are crucial optical parameters for optical fibers. The V-number of a PCF can be calculated by the following formula [49–52]:

$$V_{\text{PCF}} = \frac{2\pi\Lambda}{\lambda} \sqrt{n_{\text{core}}^2(\lambda) - n_{\text{neff}}^2(\lambda)} \tag{2}$$

Equation (2) reveals that achieving single-mode operation endlessly in a photonic crystal fiber (PCF) depends on both its geometry parameter and the propagated wavelength, where λ represents the pitch of the PCF. The single-mode cutoff criterion for a PCF is $V_{\text{PCF}} < \pi$, where n_{eff} represents the effective refractive index of the PCF’s guided mode and n_{core} represents the refractive index of its core [53, 54]. The numerical aperture means the light-gathering possibility of an optical fiber. Large NA indicates more light-gathering capability of a thread. For PCF, NA can be calculated using the following formula [55, 56]:

$$\text{NA} = \sqrt{n_{\text{core}}^2(\lambda) - n_{\text{neff}}^2(\lambda)} \tag{3}$$

The wavelength sensitivity applying wavelength integration (WI) method can be determined by the accompanying equation as follows [57, 58]:

$$S_\lambda = \frac{\Delta\lambda_{\text{peak}}}{\Delta n_a} (\text{nm/RI}) \tag{4}$$

where $\Delta\lambda_{\text{peak}}$ and Δn_a is the difference of wavelength peak shifts and analyte RI variation, respectively.

There are some interesting PCF sensor parameters such as the figure of merit (FOM), signal-to-noise ratio (SNR), and detection limit (n) closely related to the full width at half maxima (FWHM) of the loss spectra and can be calculated using the following equations [59, 60]:

$$\text{FOM} = \frac{S_\lambda}{\text{FWHM}} \tag{5}$$

$$\text{SNR} = \frac{\Delta\lambda_{\text{peak}}}{\text{FWHM}} \tag{6}$$

where FWHM is the transmittance spectrum’s full width at half-maximum.

The ability to identify the smallest change in the RI of the analyte is called the resolution, and then the following relation can be used [61, 62]:

$$R = \Delta n_a \frac{\Delta\lambda_{\text{min}}}{\Delta\lambda_{\text{peak}}} (\text{RIU}^{-1}) \tag{7}$$

where $\Delta\lambda_{\text{min}}$ is the minimum spectral resolution, assumed to be 0.1.

PCF-based SPR sensors’ working principle is based on the evanescent wave. An electromagnetic wave would partially penetrate the cladding region by propagating a beam of photons through the core. In PCF-SPR sensors, an evanescent wave extends to the cladding area, interacting with the plasma metal surface, excited free electrons

on the surface. When the frequencies of the evanescent wave align with those of free electrons on the surface, the resonance occurs, generating a surface plasma wave. This wave propagation is along the interface between metal and dielectric surfaces. This phenomenon, referred to as the resonance condition, gives rise to a distinctive narrow-band loss peak highly responsive to the properties of the adjacent dielectric medium adjoining the metal layer. The resonance is achieved when the real part of the effective refractive index (n_{eff}) of the core mode overlaps with the values of the (SPR). The maximum energy is transferred from the core to SPR mode during the resonance [63, 64]. Due to the change of refractive index of the dielectric medium (sample), n_{eff} of SPP changes results in the reducing resonance peak and shift in resonance wavelength. This indicates that the phase-matching wavelength is altered depending on the refractive index of the sample/analyte (glucose solution). The concentration of a sample can be detected by observing the variation of loss in peak due to the change of the analyte's refractive index. The following equation describes the principle of the red or blue shift [65, 66]:

$$d_p = \frac{1}{k\beta} = \frac{\lambda}{2\pi\beta} \quad (8)$$

In this context, the d_p symbol denotes the depth of penetration that the evanescent wave produces. Furthermore, the symbols β and k refer to the decay constant and wave number, respectively. Based on the equation, it may be inferred that the incident wavelength exhibits direct proportionality with d_p . Therefore, it can be observed that longer wavelengths result in higher values of d_p , whereas shorter wavelengths correspond to lower values of d_p . High coupling is evident when the core-guided and plasmonic modes exhibit a significant interaction, particularly at longer wavelengths. This interaction leads to a relatively higher level of damping for the evanescent wave. Hence, the occurrence of the red shift phenomenon can be observed. Conversely, the blue shift can occur for the opposite reason. By changing the refractive index of the environmental bio-targets surrounding the PCF, the unknown analytes can be detected by analyzing the output loss spectrum of the computer [67, 68].

This paper proposes a more realistic and practical PCF-SPR biosensor for refractive index sensing. The reported RI sensor was used for glucose concentration detection, where the analyte refractive index changes with the glucose concentration within the studied RI range. Gold and silver nanolayers are used in PCF-SPR sensors due to their unique optical properties, which are chemically stable and show the large resonance peak that makes them work better. The nanolayer and the sensing layer are put on the

outside of the fiber structure to avoid problems with liquid getting in and metal coating. The analyte can flow through or drip on the nanolayer's outer surface thanks to the external sensing layer. The proposed sensor introduces a new technique to increase the sensitivity of PCF based on nanoparticles. Finally, the sensitivity of the gold-coated PCF-SPR sensor is compared to the silver-coated PCF sensor [69, 70].

Experimental methodology

The experimental setup for the proposed glucose sensor is shown in Fig. 1, which includes using two SMFs, each 10 cm long, joined with two ends of PCF 5 cm long. This PCF has a 12- μm core diameter, an outer clad diameter of 125 μm , and a diameter of 250 outer coatings. The central region of PCF was partially removed by 0.5 cm long. After that, this region was coated with a 50 nm layer of nanomaterials to create the sensor region. Surface plasma resonance (SPR) occurs within this sensor area when interacting with certain analytes. A laser source is used with a 1550 to 1600 nm wavelength to propagate light through fiber optics. The laser beam is propagated through the SMF-PCF sensor. It is modulated by the external environmental solutions in the sensing region when the sensor is immersed in a glucose solution. The SPR phenomenon varies the characteristics of the light signal, which is later analyzed using an optical spectrum analyzer (OSA). After that, received data are processed on a computer, allowing for real-time observation and analysis of any changes in the signal. These changes refer to changes in the refractive index within the sensor area, which provides useful information about the concentration of the analyte. Accurate detection of highly sensitive materials can be achieved, making this approach particularly valuable in different applications, including chemical analysis and environmental monitoring [71, 72].

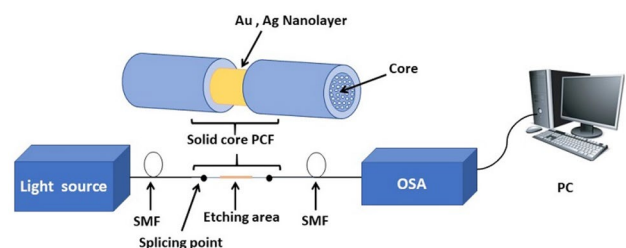


Fig. 1 The Experimental setup of PCF biosensor based on nanomaterial structure

The PCF sensor preparation procedure

Two equal-length single-mode optical fibers (SMF-28) were adopted. The SMFs used had a mode field diameter (MFD) of approximately 10 μm and a core diameter of 8.4 μm at 1550 nm and a numerical aperture of 10.4 μm at 1550 nm. The single-mode cutoff is at ≈ 1260 nm. The most important component was a photonic crystal fiber (ESM-12B) made by NKT Photonics that has always been an endless single-mode fiber with 12 ± 0.5 μm core diameter, coating diameter 245 ± 10 μm, and 125 ± 5 μm outer diameter, 7.8 μm pitch constant and 3.1 μm air hole diameter. The optical properties of (PCF) are integral to their performance. The mode field diameter is 10 ± 1 μm at a wavelength of 1550 nm. These parameters determine the spatial distribution of the guided mode within the fibers. The numerical aperture (NA) measured at 1550 nm is 0.1 ± 0.05, providing insight into the fibers' ability to collect and focus light. Additionally, the attenuation levels at various wavelengths are noteworthy at 1550 nm, and the attenuation loss is less than 1 dB/km, indicating a minimum loss of signal across distance. PCF design

contributes significantly to its sensitivity to the changes in the refractive index and its suitability for glucose sensing. This sensitivity is due to its microscopic structure, allowing light confinement and interaction with the surrounding environment. PCF also supports multiple optical conditions and changes in the refractive index allowing for the detection of accurate differences in solution concentration. The length of the resonance wave can also be adjusted to improve the sensor's response to certain analyses. In short, the design properties of PCF make it quite appropriate for glucose sensing and analysis applications [73, 74].

In this study, the PCF piece was etched by immersion in an aqueous hydrofluoric acid (HF) with a concentration of around 48%. The PCF piece appeared in the cylindrical quartz material, which was employed to encapsulate the etching solution acid. Fujikura (FSM-70 s) fusion splicing machine was used to splice the fibers. The parameters of the fusion splicer machine were carefully adjusted to maintain optimal splicing conditions. To measure the length of the air holes collapsed region Fig. 2, an optical microscope OLYMPUS BX60M supported with a high-resolution digital

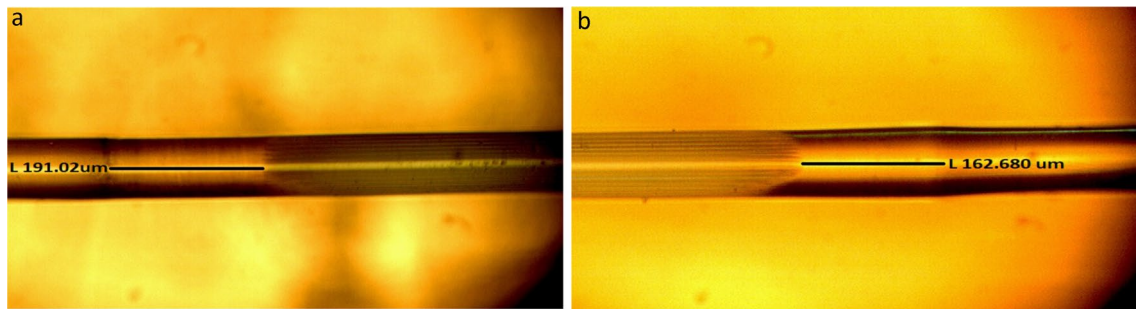


Fig. 2 Microscopic image of the splice regions between PCF (ESM-12 B) & SMF- 28 **a** the collapsed length is ~ 191.02 μm, and **b** collapsed length is ~ 162.68 μm

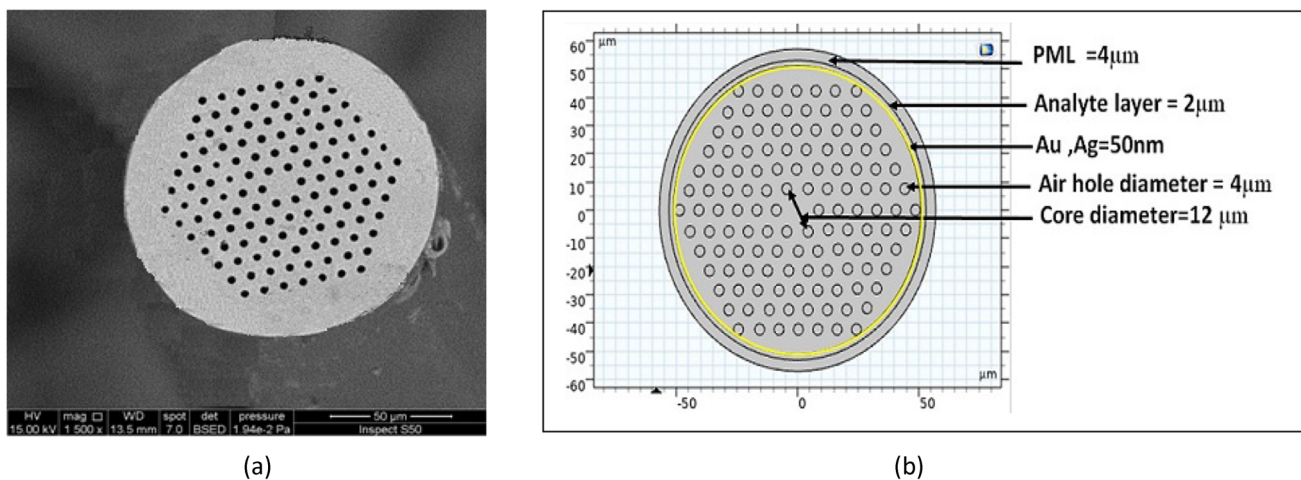


Fig. 3 **a** The cross-sectional SEM image for the employed PCF (ESM-12B) **b** the geometry design of PCF

camera was used. Figure 2 illustrates the optical microscope image of PCF etched and spliced with SMF. Figure 3a shows a scanning electron microscope (SEM) image of a fabricated (ESM-12) PCF with a pitch constant of $7.8 \mu\text{m}$ and an air hole diameter of $3.2 \mu\text{m}$ [75, 76].

Outside coating of the PCF has been suggested to overcome the inner metal coating and liquid-analyte infiltration into the air holes. The sensing mechanism is more convenient because of the metal nanolayer placement and the sensing medium outside the fiber structure. The central surface of the fiber is coated with a gold, silver of (50 nm) layer thickness using a Sputtering coater device model (Quorum Q150R ES, UK). It can accommodate many gold or silver targets. Used (Au and Ag) with 99.99% purity, 5.6 cm diameter, and 0.5 mm thick as target material, it has a 165 mm sample chamber. The distance between the PCF and the target was 10 cm, while the coating process within the chamber was performed under pressure of 3×10^{-3} tor. The optical PCF sensor was positioned within the sputter-coated chamber and securely aligned parallel to the chosen target (either gold or silver). A nanolayer of 50 nm thickness coated the center surface of the PCF to make the PCF sensor. The gold and silver thickness was examined and selected throughout the adopted research [56, 57]. This value was also tested by COMSOL software, where the best result was obtained at a thickness of 50 nm. Figure 3b illustrates a schematic of the proposed PCF-SPR sensor, created using the Finite Element method (FEM).

Results and discussion

Figure 4 shows the electric field distributions of the fundamental and surface plasmon resonance (SPR) modes obtained using COMSOL software. The parameters for the used fiber, the wavelength, and the selection of the

nanolayer thickness within 50 nm were entered. After obtaining the theoretical results, these parameters were used on the practical side to get the best results as realistically as possible. The sensor's performance is estimated by immersing the coated region of PCF surface in the Glucose dissolved in water and blood solution to examine change in the solutions' refractive indices. Several solutions were prepared, and their refractive indices were measured and considered as a reference for the sensing process. Glucose concentrations were tested in water and blood samples to evaluate the performance and sensitivity of a PCF-based glucose sensor. Water samples had glucose concentrations ranging from 80 mg/dL to 600 mg/dL, while blood samples had concentrations ranging from 89 mg/dL to 611 mg/dL. These ranges were chosen to cover a wide spectrum of glucose levels in clinical and physiological contexts. The lower limit represents normal fasting blood glucose levels, while the upper limit accounts for elevated glucose concentrations, often seen in individuals with diabetes or during post-meal periods. The chosen concentration ranges aim to assess the sensor's accuracy, sensitivity, and reliability in detecting glucose concentrations relevant to healthy individuals and those with glucose metabolism disorders. This comprehensive evaluation ensures the sensor's potential application in diabetes management and healthcare monitoring. The linear relationship between RI and solution concentration is depicted in Fig. 5.

The sensing process was conducted using a PCF sensor of 0.5 cm length, the thickness of the coated metal nanolayer was 50 nm, and RI values in the range (1.333–1.3342) for glucose dissolved in water and (1.3473–1.3502) for glucose dissolved in blood serum. The spectra were plotted by recording the transmission light curves (T) through the optical fiber. When the incident photon energy is transferred to the nanometal's electrons, it is observed that the transmittance intensity decreases with reflected light.

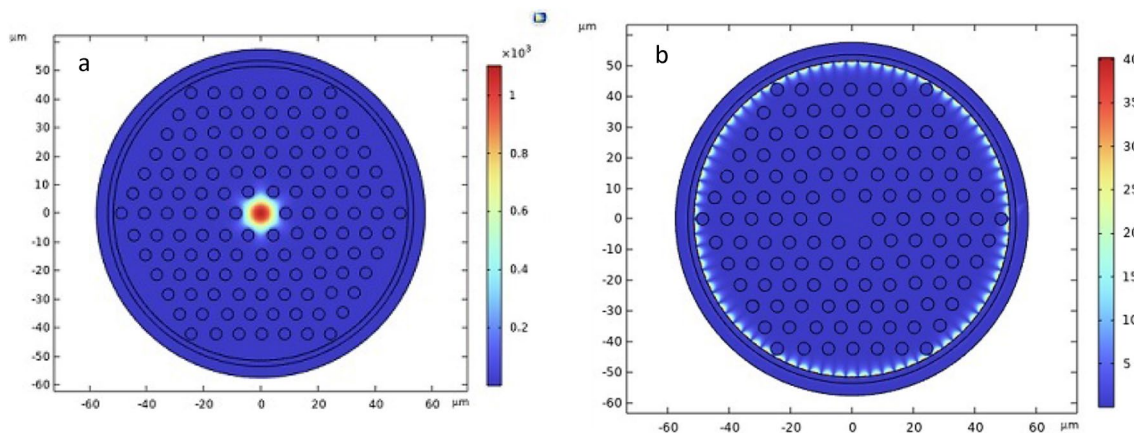


Fig. 4 The electric field distributions **a** Core mode and **b** Plasmonic mode

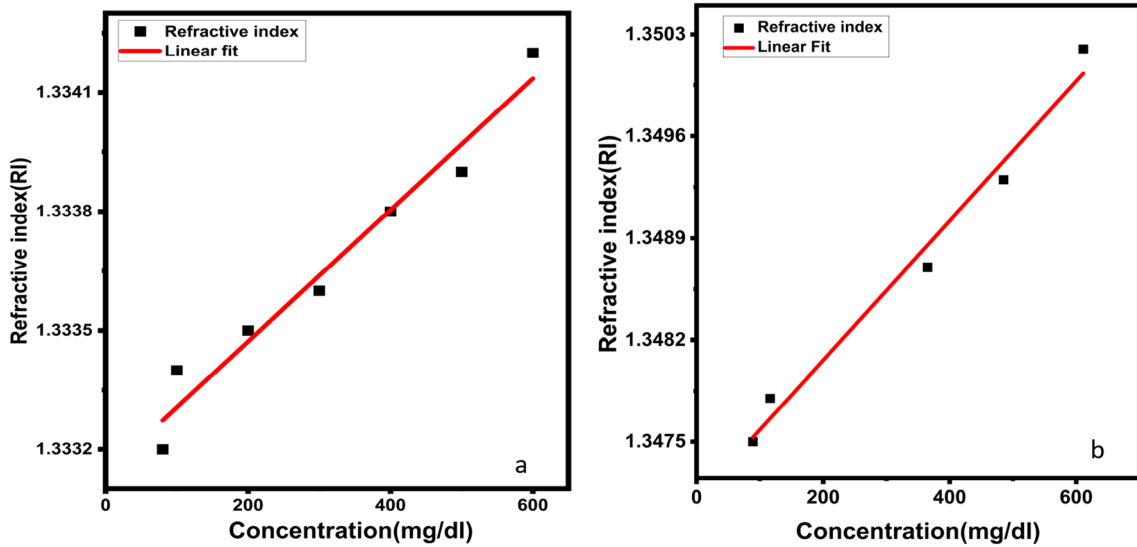
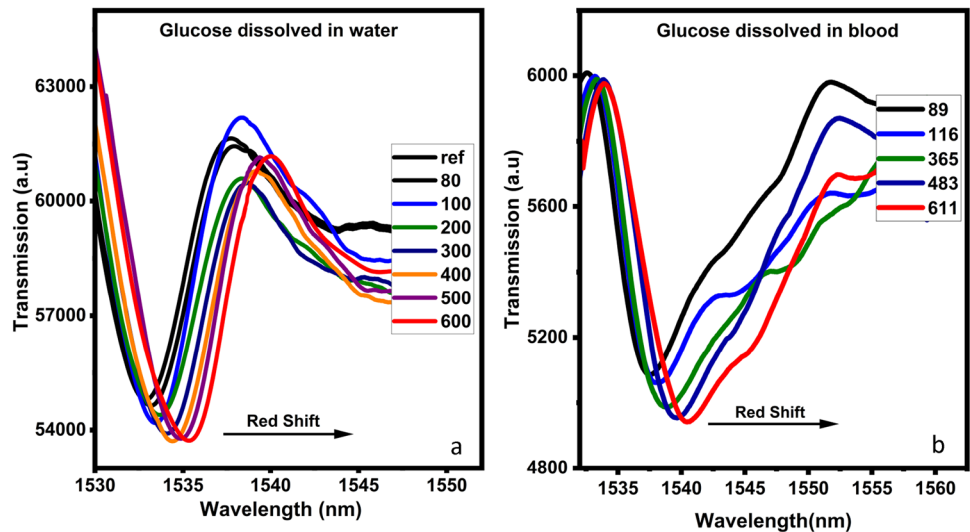


Fig. 5 The RI for **a** glucose dissolved in water solutions and **b** glucose dissolved in blood as a function of the concentration

Fig. 6 SPR curves of different concentration of glucose dissolved in **a** water and **b** in blood at the PCF coating by gold nanolayer



The λ_{res} increases as the RI of the sensor medium increase. It is generated from the resonance between the SPR wave and the incident light. Moreover, as the energy level declines, sharp dip in the λ_{res} shifts to longer wavelength (red shift). Figure 6a and b shows that the resonance wavelength of the PCF sensor coated with gold nanolayer shifts to the higher wavelength when the concentration of glucose dissolved in water and blood serum is increased.

Figure 7a and b shows that the resonance wavelength of the PCF sensor coating by silver nanolayer also shifts to the higher wavelength when glucose concentration is increased.

Fig. 8a, b shows that the glucose dissolved in water and blood solubility sensitivity of the sensor can reach 1943.72 nm/RIU and 1114.16 nm/RIU for PCF coated with gold nanolayer, respectively.

Figure 9a, b shows that the glucose dissolved in water and blood sensitivity of the sensor can reach 1892.18 nm/RIU and 1012.36 nm/RIU for PCF coated with silver through the linear fitting. To evaluate the overall performance of a sensor, FOM is defined as the ratio of sensitivity to the (FWHM). The FOM should be as high as possible to achieve a high-performance sensor, which can be obtained when the sensitivity increases and FWHM decreases.

Figure 10a, b depicts the changing of FOM and SNR values with analyte refractive index. The sensor displays highest value of FOM (644 RIU^{-1}) for the gold-based sensor and (629 RIU^{-1}) for the silver-based sensor. Also, the FOM for the glucose sensor shows a downward behavior with highest value of FOM for blood glucose for gold and silver-based sensor are (321 RIU^{-1}) and (299 RIU^{-1}), respectively, as

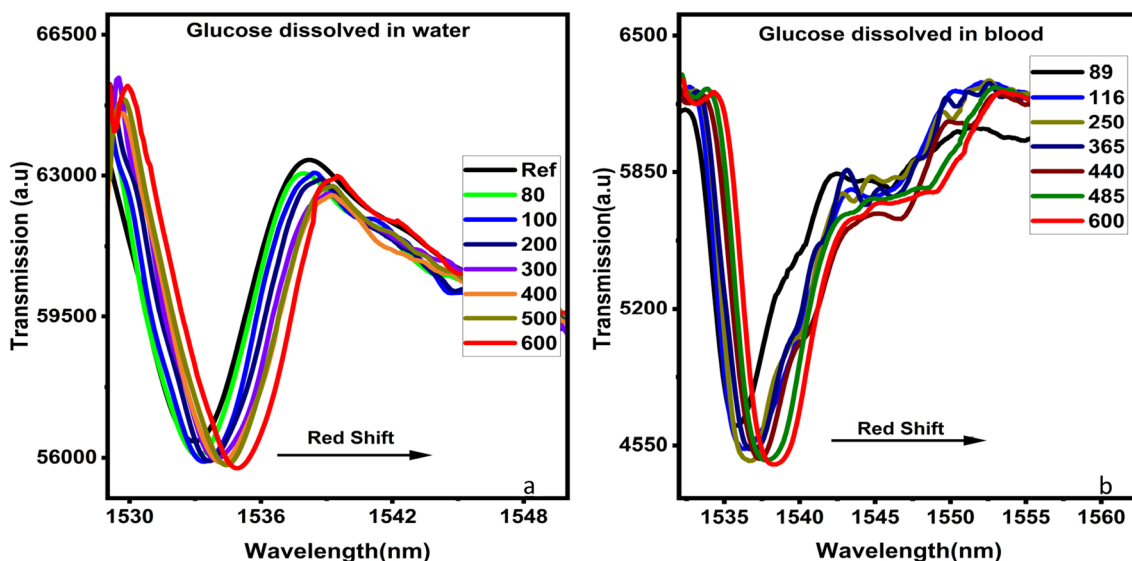


Fig. 7 SPR curves of different concentration of glucose dissolved in a water and b blood at the PCF coating silver nanolayer

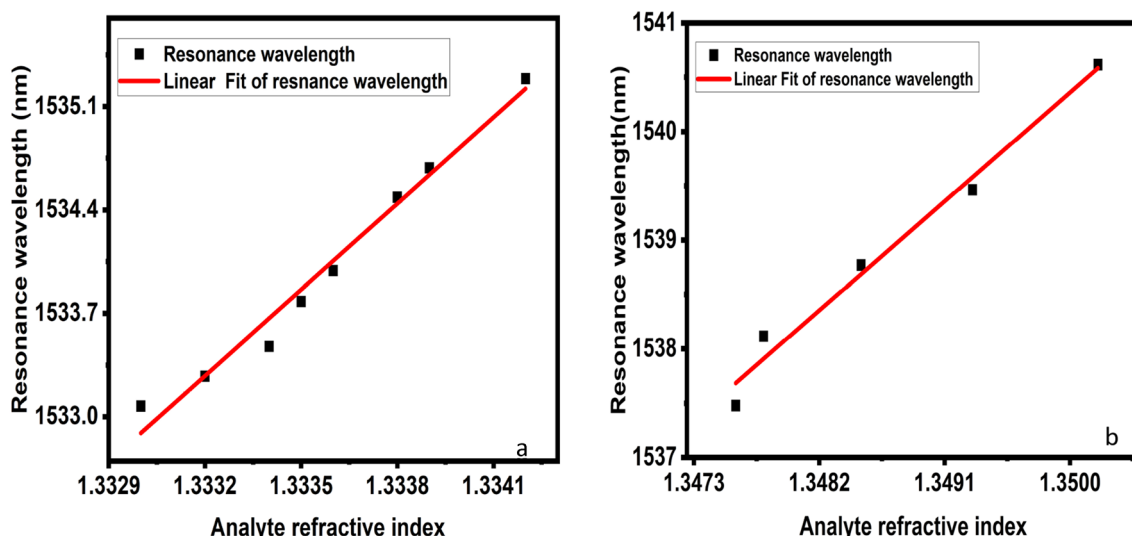


Fig. 8 Variation of SPR resonance wavelength of different refractive index for glucose dissolved in a water and b in blood, for the PCF coating by gold nanolayer

shown in Fig. 10a, b. The second important parameter is SNR, which is calculated using Eq. 6. The maximum SNR values for glucose in water is 0.13, and 0.06 for glucose in blood for gold-coated PCF, respectively, Fig. 10a, b. In contrast, the values of SNR for and glucose dissolved in water and blood at silver sensors are 0.108 and 0.16, respectively Fig. 11a, b. An essential parameter for determining a sensor’s detection limit is the sensor resolution.

Figures 12 and 13 show the variation of resolution values with analyte refractive index. An optimum resolution of 3.3×10^{-5} RIU was obtained for the glucose dissolved in

water when gold-based sensor was used. while 3.31×10^{-5} RIU for the glucose dissolved in water for silver-based PCF sensor and 3.34×10^{-5} RIU, 3.3×10^{-5} for glucose blood gold and silver-based sensor are obtained when $\Delta\lambda_{\min} = 0.1$ nm is considered. Therefore, this PCF-based plasmonic sensor has a good resolution for sensing the dissolved Glucose that has ever been achieved. The resolution of this PCF sensor can detect a tiny change in RI on the order of 10^{-5} .

Although the photonic crystal fiber (PCF) sensor system is highly sensitive and accurate, it is subject to different sources of error and uncertainty. Temperature fluctuations,

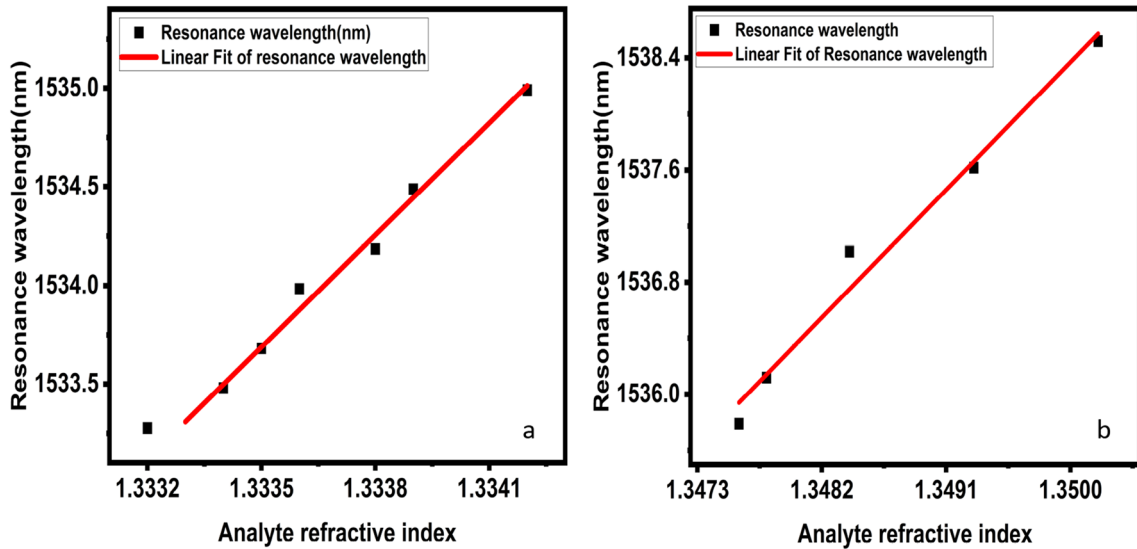


Fig. 9 Variation of SPR resonance wavelength of different refractive index for glucose dissolved **a** in water and **b** in blood, of the PCF coating by silver nanolayer

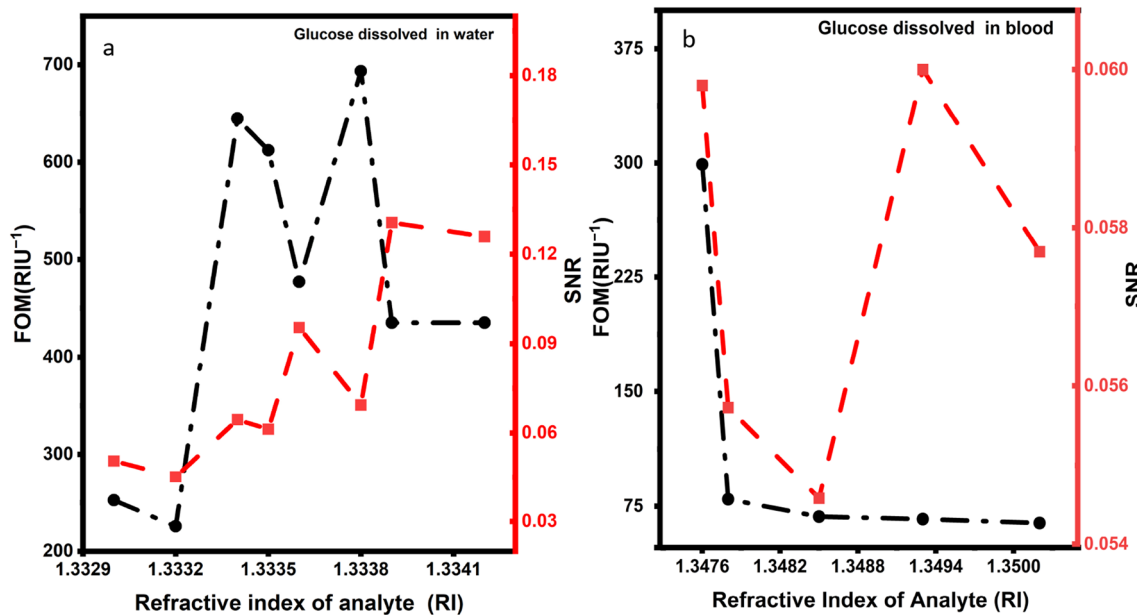


Fig. 10 FOM and SNR for different analyte refractive index **a** glucose dissolved in water and **b** glucose dissolved in the blood, at PCF coating by gold nanolayer

changes in humidity and pressure, and fluctuations in the wavelength of the light source can lead to measurement errors in addition, the efficiency of combining light within and outside PCF, signal noise, sample characteristics, calibration errors, and optical loss could contribute more to uncertainty.

Reducing these potential sources of error and uncertainty requires careful attention to experimental design, calibration, quality control, and data analysis to ensure the reliability and

accuracy of PCF sensor measurements. Minimizing potential sources of error and uncertainty has received particular attention. Correct glucose measurements are essential for medical and scientific applications. To achieve this, we have prioritized rigorous calibration for the PCF-based sensor system, providing frequent and comprehensive tests of the device’s accuracy. Environmental factors, such as temperature and humidity, were carefully controlled during our experiments to minimize their effect on measurements.

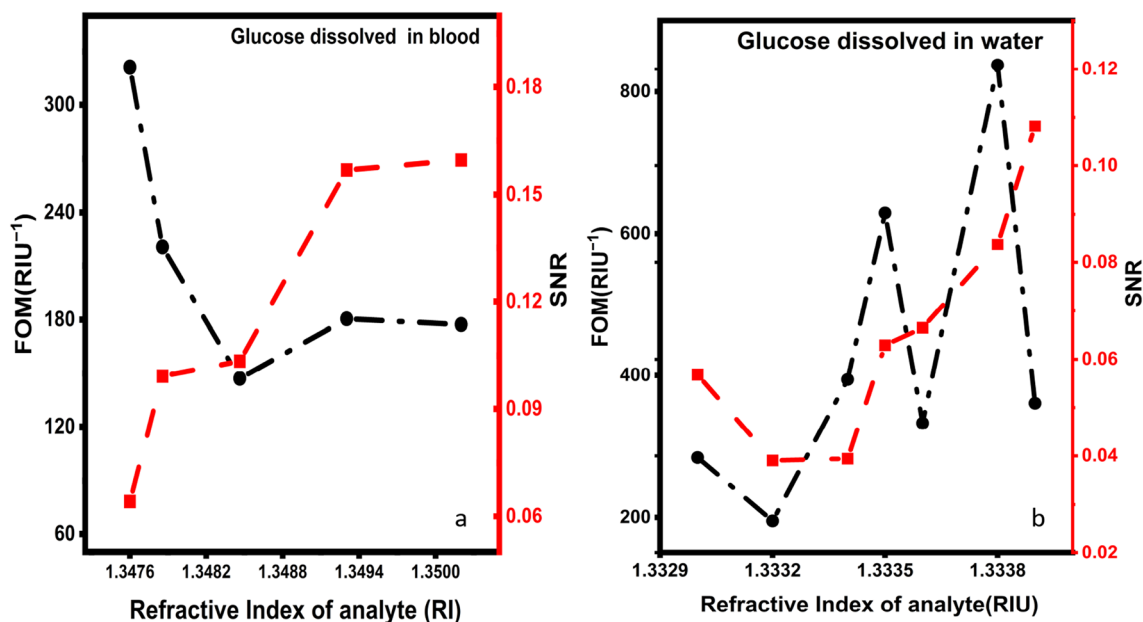


Fig. 11 FOM and SNR for different analyte refractive index **a** glucose dissolved in water and **b** glucose dissolved in blood, for PCF coating by silver nanolayer

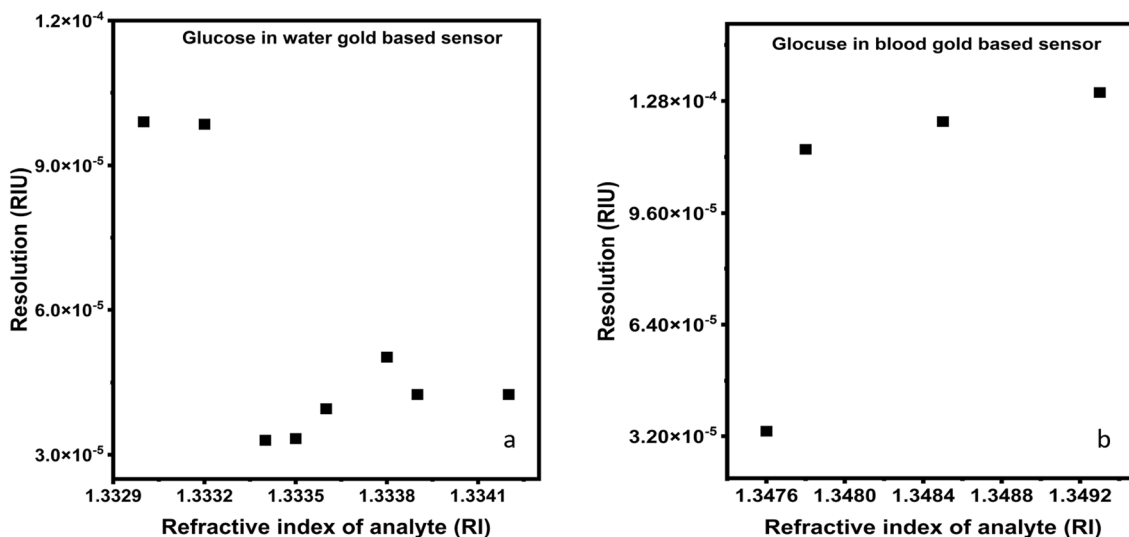


Fig. 12 The resolution for different analyte refractive index **a** glucose dissolved in water **b** glucose dissolved in blood, of the PCF coating with gold nanolayer

In addition, our study includes repeated experiments to verify the reliability of our sensor performance through multiple experiments. By implementing these measures, we aim to provide reliable results of glucose measurement that enhance glucose sensing and are helpful for medical diagnosis and treatment control.

The sensor detects glucose through specific chemical reactions, offering potential medical applications, environmental control, food safety, and biotechnology applications.

By modifying its design, it can detect vital indicators, chemicals, pollutants, toxins, and dangerous chemicals, enabling disease diagnosis and prevention. However, challenges like sensitivity, quality, and calibration methods may arise.

The sensor faces limitations in glucose concentrations, miniaturization, and operational integration. Miniaturization affects accuracy and manufacturing, while practical integration challenges like energy consumption and user interface design impact wearable devices and medical equipment.

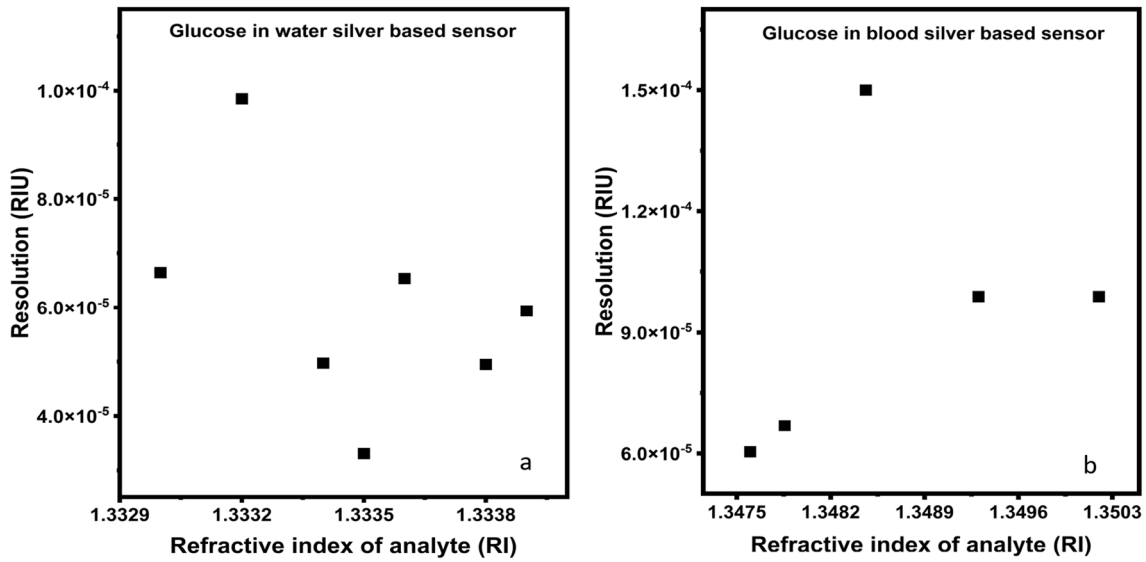


Fig. 13 The resolution for different analyte refractive index **a** glucose dissolved in water **b** glucose dissolved in blood, of the PCF coating with silver nanolayer

Continuous research and development efforts aim to expand the sensor’s capabilities and address constraints. This extended work provides transparency about the sensor’s capabilities and highlights areas for improvement.

The proposed PCB-SPR glucose sensor offers distinct advantages compared to present glucose sensing techniques. In addition to its unique optical properties, its exceptional sensitivity to changes in glucose concentration allows accurate measurements to be made even at low glucose levels. This sensitivity exceeds what is possible with conventional enzymatic methods and some emerging optical sensors. The PCF-based sensor has excellent accuracy and can detect minor changes in refractive index due to glucose concentration variance. This high accuracy is helpful for real-time observation of glucose fluctuations, an essential aspect of managing diabetes. In comparison, conventional methods, such as test strips, often have limited resolution.

The PCF-based glucose sensor provides intense sensitivity, accuracy, and non-interference, making it a promising alternative to traditional and apparent glucose sensing

techniques. However, their cost, complexity, environmental vulnerability, and calibration requirements may pose challenges in particular applications. Therefore, the choice between this sensor and current techniques must consider the patient’s needs or application requirements, considering trade-offs between performance and practical application.

We conducted a series of experiments under controlled conditions to evaluate the potential for repetition of our sensor. The results were analyzed for consistency. To evaluate our sensor’s stability, we subjected it to various environmental conditions, including temperature fluctuations and humidity changes. The sensor’s performance was continuously monitored during these tests. We realize that differences in manufacturing can affect sensor performance. These differences may include material characteristics, assembly procedures, or calibration processes. We have identified potential sources of variation and their potential effects on sensitivity and accuracy. Differences in the assembly process were found to introduce minor differences in the calibration of sensors, leading to differences in sensitivity.

Table 1 Performance Comparison previously reported and proposed PCF-SPR Sensor

Structure type	Sensitivity nm/RIU	Refractive Index Range	Resolution RIU	References
Helical intermediate-period fiber grating (HIPFG)	213.6	1.33–1.36	–	[77]
Optical fiber tip sensor	1467.59	1.364–1.397	3.4×10^{-4}	[78]
D-shaped PCF refractive index sensor	294.11	1.33–1.354	6.8×10^{-5}	[79]
Photonic crystal fiber pollution sensor	1360.2	1.33–1.362	7×10^{-5}	[80]
Gold-coated external sensing approach	1,000	1.33–1.37	8.5×10^{-5}	[81]
Silver-coated photonic crystal fiber sensor	1323	1.445–1.4454	5.66×10^{-4}	[82]
This work	1943	1.333–1.3342	3.3×10^{-5}	

To show the competitiveness of our design, we compare the proposed structure with others', which included experimental work and simulation, as shown in Table 1. Our sensor has advantages due to its high sensitivity of 1943 nm/RIU.

Conclusions

The development and evaluation of a solid-core Photonic Crystal Fiber (PCF)-based sensor based on gold and silver nanoparticles for Surface Plasmon Resonance (SPR) applications were the main goals of the study. The research offers important findings, with a maximum sensitivity of 1943.43 nm/RIU and 1892.18 nm/RIU for glucose dissolved in water, respectively. The effect of the coating layer on the sensor's performance was a major aspect of our study. By comparing the gold and silver layers, it is clear that the gold layer has resulted in significantly higher sensitivity when compared with the silver layer. Furthermore, it was noted that the resonance wavelength exhibited a red shift as the concentration of glucose increased. These results show the sensor's important to detect glucose accurately and sensitively in both glucoses dissolved in the blood and water. The red shift in resonance frequency demonstrates the sensor's capability to monitor glucose levels, which can be used to detect variations in glucose concentration.

This study advances the field of glucose sensing and lays the way for creating glucose sensors based on solid-core PCF nanoparticles. These sensors have promising uses in biomedicine and healthcare because they are enabling to monitor of glucose levels effectively.

References

- X.C. Yang, Y. Lu, B.L. Liu, J.Q. Yao, Temperature sensor based on photonic crystal fiber filled with liquid and silver nanowires. *IEEE Photon. J.* **8**(3), 6803309 (2016)
- M.A. Fakhri, E.T. Salim, R.K. Ibrahim, H.S. Ali, A.S. Azzahrani, R.A. Ismail, S.C.B. Gopinath, A.C. Kadhim, Z.T. Salim, Investigations on device structure and sensing mechanism using gold nanoparticles decorated photonic crystal fiber-based biosensors. *Plasmonics* (2023). <https://doi.org/10.1007/s11468-023-02015-4>
- S. Asaduzzaman, K. Ahmed, T. Bhuiyan, T. Farah, Hybrid photonic crystal fiber in chemical sensing. *Springerplus* **5**(1), 748 (2016)
- M.A. Fakhri, A.A. Alwahib, E.T. Salim, R.A. Ismail, H.A.A.A. Amir, R.K. Ibrahim, S.F.H. Alhasan, F.H. Alsultany, Z.T. Salim, S.C.B. Gopinath, Preparation and characterization of UV-enhanced GaN/ porous Si photodetector using PLA in liquid. *Silicon* (2023). <https://doi.org/10.1007/s12633-023-02528-x>
- V. Kaur, S. Singh, Performance analysis of multichannel surface plasmon resonance sensor with dual coating of conducting metal oxide. *J. Nanophotonics* **12**(01), 016012 (2018)
- M.A. Fakhri, E.T. Salim, G.M. Sulaiman, S. Albukhaty, H.S. Ali, Z.T. Salim, S.C.B. Gopinath, U. Hashim, Z.T. Al-aqbi, Gold nanowires based on photonic crystal fiber by laser ablation in liquid to improve colon biosensor. *Plasmonics* (2023). <https://doi.org/10.1007/s11468-023-01961-3>
- T. Zhang, Y. Zheng, C. Wang, Z. Mu, Y. Liu, J. Lin, A review of photonic crystal fiber sensor applications for different physical quantities. *Appl. Spectrosc. Rev.* **53**(6), 486–502 (2018)
- E.T. Salim, M.A. Fakhri, S.M. Tariq, A.S. Azzahrani, R.K. Ibrahim, A.A. Alwahib, S.F.H. Alhasan, A.T. Ramizy, E.Y. Salih, Z.T. Salim, The unclad single-mode fiber-optic sensor simulation for localized surface plasmon resonance sensing based on silver nanoparticles embedded coating. *Plasmonics* (2023). <https://doi.org/10.1007/s11468-023-01949-z>
- A.A. Rifat, G.A. Mahdiraji, R. Ahmed, D.M. Chow, Y.M. Sua, Y.G. Shee, F.R.M. Adikan, Copper-graphene-based photonic crystal fiber plasmonic biosensor. *IEEE Photon. J.* **8**(1), 1–8 (2016)
- M.A. Fakhri, E.T. Salim, S.M. Tariq, R.K. Ibrahim, F.H. Alsultany, A.A. Alwahib, S.F.H. Alhasan, S.C.B. Gopinath, Z.T. Salim, U. Hashim, A gold nanoparticles coated unclad single mode fiber-optic sensor based on localized surface plasmon resonance. *Sci. Rep.* **13**, 5680 (2023)
- V. Kaur, S. Singh, Design of titanium nitride coated PCF-SPR sensor for liquid sensing applications. *Opt. Fiber Technol.* **48**, 159–164 (2019)
- R.A. Ismail, E.T. Salim, M.S. Alwazny, Nanosecond laser ablation of Au@LiNbO₃ core-shell nanoparticles in ethanol: properties and application in optoelectronic devices. *Plasmonics* **18**(2), 561–576 (2023)
- A.K. Paul, M.A. Mollah, M.Z. Hassan, N. Gomez-Cardona, E. Reyes-Vera, Graphene-coated highly sensitive photonic crystal Fiber surface Plasmon resonance sensor for aqueous solution: design and numerical analysis. *Photonics* **8**(5), 155 (2021)
- S. Osamah, A.A. Alwahib, M.A. Fakhri, S.C.B. Gopinath, Study of single and symmetrical D-shaped optical fiber sensor based on gold nanorods. *J. Opt.* **5**, 96 (2023)
- A.A. Rifat, K. Ahmed, S. Asaduzzaman, B.K. Paul, R. Ahmed, Development of photonic crystal fiber-based gas/chemical sensors. *Comput. Photon. Sens.* (2019). https://doi.org/10.1007/978-3-319-76556-3_12
- N.K. Hassan, F.G. Khalid, A.A. Ekshayesh, O.S. Dahham, M.M. Hussein, Optical investigations of gold nano rods and gold nano rods doped with ZnO nanoparticles for optoelectronic applications. *J. Opt.* (2023). <https://doi.org/10.1007/s12596-023-01120-1>
- J.L.U. Unjie, Y.L.I. An, Y.A.H. An, Y.I.L. Iu, J.I.G. Ao, D-shaped photonic crystal fiber plasmonic refractive index sensor based on gold grating. *Appl. Opt.* **57**(19), 5268–5272 (2018)
- S.M. Tariq, M.A. Fakhri, Design and simulation of optical fibre based of gold nanoparticles for sensor applications. *Int. J. Nanoelectron. Mater.* **15**, 59–70 (2022)
- Q. Liu, S. Wang, H. Mu, Y. Sun, J. Zhao, K. Wang, W. Liu, J. Lv, P. K. Chu, C. Liu, Surface plasmon resonance sensor composed of a D-type photonic crystal fiber with a three-layer coating. *J. Opt. Soc. Am. A.* **40**(7), 1352–1358 (2023).
- M.J. Abd-ALhussain, B.G. Rasheed, M.A. Fakhri, Review on photonic crystal fiber-based nanoparticle for sensing applications. *Int. J. Nanoelectron. Mater.* **15**, 71–79 (2022)
- Z. Fan, Surface plasmon resonance refractive index sensor based on photonic crystal fiber covering nano-ring gold film. *Opt. Fiber Technol.* **50**, 194–199 (2019)
- D.A. Resen, M.F. Mohammed, M.A. Fakhri, Review of recent optical bio-sensor based FBG. *Int. J. Nanoelectron. Mater.* **15**, 165–181 (2022)
- W.L. Ng, A.A. Rifat, W.R. Wong, G.A. Mahdiraji, F.R.M. Adikan, A novel diamond ring fiber-based surface plasmon resonance sensor. *Plasmonics* **13**(4), 1165–1170 (2018)
- T.E. Abdulrahman, R.O. Mahdi, E.T. Salim, Synthesis of Nb₂O₅ nanoparticle by liquid phase laser ablation method. *Int. J. Nanoelectron. Mater.* **15**, 13–25 (2022)

25. T. Li, L. Zhu, X. Yang, X. Lou, L. Yu, A refractive index sensor based on h-shaped photonic crystal fibers coated with ag-graphene layers. *Sensors (Switzerland)* **20**(3), 741 (2020). <https://doi.org/10.3390/s20030741>
26. M.S. Muhsin, J.A. Saimon, E.T. Salim, Incorporation of metal nanoparticle to enhance tungsten oxide (WO₃) films properties: a mini review. *Int. J. Nanoelectron. Mater.* **15**, 111–118 (2022)
27. X. Chen, L. Xia, C. Li, Surface plasmon resonance sensor based on a novel D-shaped photonic crystal fiber for low refractive index detection. *IEEE Photon. J.* **10**(1), 6800709 (2018)
28. H.A.A.A. Amir, M.A. Fakhri, A.A. Alwahib, Synthesized of GaN nanostructure using 1064 nm laser wavelength by pulsed laser ablation in liquid. *Eng. Technol. J.* **40**(2), 404–411 (2022)
29. J.K. Nayak, P. Parhi, R. Jha, Graphene oxide encapsulated gold nanoparticle based stable fibre optic sucrose sensor. *Sens. Actuat. B Chem.* **221**, 835–841 (2015)
30. N.K. Hassan, M.A. Fakhri, E.T. Salim, Physical properties of pure gold nanoparticles and gold doped ZnO nanoparticles using laser ablation in liquid for sensor applications. *Eng. Technol. J.* **40**(2), 422–427 (2022)
31. L. Singh, R. Singh, B. Zhang, B.K. Kaushik, S. Kumar, Localized surface plasmon resonance based hetero-core optical fiber sensor structure for the detection of L-cysteine. *IEEE Trans. Nanotechnol.* **19**, 201–208 (2020)
32. T.E. Abdulrahman, E.T. Salim, R.O. Mahdi, M.H.A. Wahid, Nb₂O₅ nano and microspheres fabricated by laser ablation. *Adv. Nat. Sci: Nanosci. Nanotechnol.* **13**, 045006 (2022)
33. T. Guo, Fiber grating-assisted surface plasmon resonance for biochemical and electrochemical sensing. *J. Light. Technol.* **35**(16), 3323–3333 (2017)
34. S. Osamah, A. A. Alwahib and M. A. Fakhri, D-shape optical fibers based on gold nanoparticles for a different sensors: a review, in AIP Conference Proceedings, 2660, 020135 (2022); <https://doi.org/10.1063/5.0107768>
35. M.R. Hasan, M.A. Islam, A.A. Rifat, A single mode porous-core square lattice photonic crystal fiber for THz wave propagation. *J. Eur. Opt. Soc.* **12**, 15 (2016)
36. S.M. Tariq, M.A. Fakhri, E.T. Salim, U. Hashim, F.H. Alsultany, Design of an unclad single-mode fiber-optic biosensor based on localized surface plasmon resonance by using COMSOL Multiphysics 5.1 finite element method. *Appl. Opt.* **61**(21), 6257–6267 (2022)
37. D.J.J. Hu, H.P. Ho, Recent advances in plasmonic photonic crystal fibers: design, fabrication and applications. *Adv. Opt. Photon.* **9**(2), 257 (2017)
38. M.S. Alwazny, R.A. Ismail, E.T. Salim, Aggregation threshold for Novel Au–LiNbO₃ core/shell Nano composite: effect of laser ablation energy fluence. *Int. J. Nanoelectron. Mater.* **15**(3), 223–232 (2022)
39. K. Tsuruda, M. Fujita, T. Nagatsuma, Extremely low-loss terahertz waveguide based on silicon photonic-crystal slab. *Opt. Express.* **23**, 31977–31990 (2015)
40. M.S. Alwazny, R.A. Ismail, E.T. Salim, High-quantum efficiency of Au@LiNbO₃ core-shell nano composite as a photo-detector by two-step laser ablation in liquid. *Appl. Phys. A* **128**, 500 (2022)
41. M.M. Rahman, M.M. Rana, M.S. Anower, M.S. Rahman, A.K. Paul, Design and analysis of photonic crystal fiber-based plasmonic microbiosensor: an external sensing scheme. *SN Appl. Sci.* **2**, 1194 (2020)
42. A.D. Faisal, W.K. Khalef, E.T. Salim, F.H. Alsultany, M.H.A. Wahid, Conductivity modification of ZnO NRs films via gold coating for temperature sensor application. *Key Eng. Mater.* **936**, 105–114 (2022)
43. M.M.A. Eid, M.A. Habib, M.S. Anower, A.N.Z. Rashed, Highly sensitive nonlinear photonic crystal fiber based sensor for chemical sensing applications. *Microsyst. Technol.* **27**(3), 1007–1014 (2021)
44. N.K. Hassan, M.A. Fakhri, A.W. Abdulwahhab, U. Hashim, Preparation of gold nanoparticles doped zinc oxide using reactive pulsed laser ablation in liquid. *Key Eng. Mater.* **911**, 65–76 (2022)
45. W.Y.A.W. Luo, X.B. Li, S.A.A. Abbasi, S.A. Zhu, H.-P.A. Ho, Analysis of the D-shaped PCF-based SPR sensor using resonance electron relaxation and fourier domain method. *Opt. Lasers Eng.* **166**, 107588 (2023)
46. S.M. Tariq, M.A. Fakhri, U. Hashim, Fiber optics for sensing applications in a review. *Key Eng. Mater.* **911**, 65–76 (2022)
47. L. Duan, X. Yang, Y. Lu, J. Yao, Hollow-fiber-based surface plasmon resonance sensor with large refractive index detection range and high linearity. *Appl. Opt.* **56**(36), 9907 (2017)
48. H.S. Ali, M.A. Fakhri, Z. Khalifa, Optical and structural properties of the gold nanoparticles ablated by laser ablation in ethanol for biosensors. *J. Phys: Conf. Ser.* **1795**(1), 012065 (2021)
49. T.S.Y. Feng, W. Zhang, T. Xu, L. Huang, C. Liu, D-shaped photonic crystal fiber sensor based on the surface plasmon resonance effect for refractive index detection. *Appl. Opt.* **62**(16), E83–E91 (2023)
50. M.A. Hassan, B.M. Al-Nedawe, M.A. Fakhri, Embedded optical fiber link interferometer sensors for snapshot surface inspection using the synthetic wavelength technique,". *Appl. Opt.* **60**(8), 2339–2347 (2021)
51. M. De, T.K. Gangopadhyay, V.K. Singh, Prospects of photonic crystal fiber as physical sensor: an overview. *Sensors (Switzerland)* **19**(3), 464 (2019)
52. N.K. Hassan, M.A. Fakhri, E.T. Salim, M.A. Hassan, Gold nanoparticles based optical fibers for a different sensor in a review. *Mater. Today Proc.* **42**, 2769–2772 (2021)
53. A.A. Rifat, K. Ahmed, S. Asaduzzaman, B.K. Paul, R. Ahmed, Development of photonic crystal fiber based gas/chemical sensors, in *Computational Photonic Sensors*. ed. by M. Hameed, S. Obayya (Springer, Cham, 2019)
54. A.D. Faisal, R.A. Ismail, W.K. Khalef, E.T. Salim, Synthesis of ZnO nanorods on a silicon substrate via hydrothermal route for optoelectronic applications. *Opt. Quant. Electron.* **52**, 1–12 (2020)
55. B.K. Paul, F. Ahmed, M.G. Moctader, K. Ahmed, D. Vigneeswaran, Silicon nano crystal filled photonic crystal fiber for high nonlinearity. *Opt. Mater. (Amst)* **84**, 545–549 (2018)
56. H.S. Ali, M.A. Fakhri, An overview of Au & Photonic crystal fiber of sensors. *Mater. Sci. For.* **1002**, 282–289 (2020)
57. E.K. Akowuah, T. Gorman, H. Ademgil, S. Haxha, G.K. Robinson, J.V. Oliver, Numerical analysis of a photonic crystal fiber for biosensing applications. *IEEE J. Quant. Electron.* **48**(11), 1403–1410 (2012)
58. S.A. Adnan, Z.H. Tawfiq, M.A. Fakhri, Gold nanoparticles in liquid based on photonic crystal fiber PCF for sensors application. *Defect Diffus. Forum* **398**, 23–28 (2020)
59. M.S.A. Gandhi, K. Senthilnathan, P.R. Babu, Q. Li, Visible to near infrared highly sensitive microbiosensor based on surface plasmon polariton with external sensing approach results in physics visible to near infrared highly sensitive microbiosensor based on surface plasmon polariton with external sensing. *Res. Phys.* **15**, 102590 (2019)
60. H.T. Halboos, E.T. Salim, Silver doped niobium pentoxide nanostructured thin film, optical structural and morphological properties. *IOP Conf. Ser. Mater. Sci. Eng.* **454**(1), 012174 (2018)
61. H. Yang et al., Highly sensitive graphene-au coated plasmon resonance PCF sensor. *Sensors (Switzerland)* **21**(3), 1–14 (2021). <https://doi.org/10.3390/s21030818>
62. M.A. Fakhri, E.T. Salim, M.H.A. Wahid, A.W. Abdulwahhab, Z.T. Salim, U. Hashim, Heat treatment assisted-spin coating

- for LiNbO₃ films preparation: their physical properties. *J. Phys. Chem. Solids* **131**, 180–188 (2019)
63. M. N. Sakib and M. S. Anower, Designing and Characterizing a Multi-core PCF SPR Biosensor, in 3rd IEEE International Conferences Telecommunication Photonics, ICTP 2019, 1–4 (2019)
 64. M.A. Fakhri, E.T. Salim, M.H.A. Wahid, A.W. Abdulwahhab, U. Hashim, Z.T. Salim, Efficiency enhancement of optical strip waveguide by the effect of heat treatment. *Optik* **180**, 768–774 (2019)
 65. N.H.H.M. Al Mahfuz, Md.. A. Hossain, E. Haque, Y. Namihira, F. Ahmed, A bimetallic-coated, low propagation loss, photonic crystal fiber based plasmonic refractive index sensor Mohammad. *Sensors* **19**(17), 3794 (2019)
 66. E.T. Salim, J.A. Saimon, M.K. Abood, M.A. Fakhri, Effect of ammonium concentration on structural, optical and morphological properties of H-Nb₂O₅ thin films-A novel study. *Mater. Res. Express* **6**(4), 046420 (2019)
 67. M.K. Abood, M.H.A. Wahid, J.A. Saimon, E.T. Salim, Physical properties of Nb₂O₅ thin films prepared at 12M ammonium concentration. *Int. J. Nanoelectron. Mater.* **11**, 237–244 (2018)
 68. M.A. Fakhri, E.T. Salim, A.W. Abdulwahhab, U. Hashim, Z.T. Salim, Optical properties of micro and nano LiNbO₃ thin film prepared by spin coating. *Opt. Laser Technol.* **103**, 226–232 (2018)
 69. Z.H. Tawfiq, M.A. Fakhri, S.A. Adnan, Photonic crystal fibres PCF for different sensors in review. *IOP Conf. Ser. Mater. Sci. Eng.* **454**(1), 012173 (2018). <https://doi.org/10.1088/1757-899X/454/1/012173>
 70. M.A. Fakhri, E.T. Salim, M.H.A. Wahid, U. Hashim, Z.T. Salim, Optical investigations and optical constant of nano lithium niobate deposited by spray pyrolysis technique with injection of Li₂CO₃ and Nb₂O₅ as raw materials. *J. Mater. Sci. Mater. Electron.* **29**(11), 9200–9208 (2018)
 71. M.K. Abood, E.T. Salim, J.A. Saimon, Niobium pentoxide thin film prepared using simple colloidal suspension for optoelectronic application. *Int. J. Nanoelectron. Mater.* **11**(2), 127–134 (2018)
 72. S.A. Naayi, A.I. Hassan, E.T. Salim, FTIR and X-ray diffraction analysis of Al₂O₃ nanostructured thin film prepared at low temperature using spray pyrolysis method. *Int. J. Nanoelectron. Mater.* **11**, 1–6 (2018)
 73. M.K. Abood, E.T. Salim, J.A. Saimon, Impact of substrate type on the microstructure of H-Nb₂O₅ thin film at room temperature. *Int. J. Nanoelectron. Mater.* **11**, 55–64 (2018)
 74. E.T. Salim, Surface morphology and X-ray diffraction analysis for silicon nanocrystal-based heterostructures. *Surf. Rev. Lett.* **20**(05), 1350046 (2013)
 75. M.K. Abood, M. Halim, A. Wahid, E.T. Salim, J. Admon, Niobium Pentoxide thin films employ simple colloidal suspension at low preparation temperature. *Eur. Phys. J. Conf.* **162**(12), 01058 (2017)
 76. R.A. Ismail, E.T. Salim, W.K. Hamoudi, Characterization of nano-structured hydroxyapatite prepared by Nd:YAG laser deposition. *Mater. Sci. Eng. C* **33**(1), 47–52 (2013)
 77. J. Zhong, S. Liu, T. Zou, W. Yan, P. Chen, B. Liu, Z. Sun, Y. Wang, High-sensitivity optical fiber-based glucose sensor using helical intermediate-period fiber gratin. *Sensors* **22**(18), 6824 (2022)
 78. C.I.A. Ferreira, M.S. Ferreira, L. Pinto, C.I.A. Ferreira, M.S. Ferreira, Optical fiber tip sensor for the measurement of glucose aqueous solutions. *IEEE Photon. J.* **10**(5), 6803609 (2018)
 79. M.Y. Azab, M.F.O. Hameed, G.A. Mahdiraji, F.R.M. Adikan, S.S.A. Obayya, Experimental and numerical characterization of a D-shaped PCF refractive index sensor. *Opt. Quantum Electron.* **54**(12), 1–14 (2022)
 80. F.F. Abbas, S.S. Ahmed, Photonic crystal fiber pollution sensor based on surface plasmon resonance. *Iraqi J. Sci.* **64**(2), 658–667 (2023)
 81. F.R.M.A.A.A. Rifat, G.A. Mahdiraji, Y.G. Shee, Md.J. Shawon, A novel photonic crystal fiber biosensor using surface plasmon resonance. *Procedia Eng.* **140**, 1–7 (2016)
 82. A.I. Mahmood, S.A. Kadhim, N.F. Mohammed, I.A. Naseef, Simulation design of silver nanoparticle coated photonic crystal fiber sensor based on surface plasmon resonance. *Exp. Theor. Nanotechnol.* **5**, 57–64 (2021)

Publisher's Note Springer Nature remains neutral with regard to jurisdictional claims in published maps and institutional affiliations.

Springer Nature or its licensor (e.g. a society or other partner) holds exclusive rights to this article under a publishing agreement with the author(s) or other rightsholder(s); author self-archiving of the accepted manuscript version of this article is solely governed by the terms of such publishing agreement and applicable law.